Optimal Fuel-Image Motion Planning for a Class of Dual Spacecraft Formations

I. I. Hussein A. M. Bloch D. J. Scheeres N. H. McClamroch

***Abstract*— In this paper we study a class of dual spacecraft formations for imaging applications. After motivating the problem, we discuss the general goals of an imaging formation. We then specialize the discussion to a class of dual spacecraft formations and introduce the geometric constraints imposed on the formation. The first main contribution of this paper is that we combine two ideas introduced separately in the literature and propose a maneuver that offers improved imaging performance. We then formulate an optimal control problem to minimize fuel consumption and further maximize image quality by minimizing the relative speed, which is proportional to the signal-to-noise ratio of the reconstructed image. We use the Maximum Principle to derive the necessary optimality conditions and show that they are also sufficient and that the resulting control law is unique. Finally, we apply a continuation method to solve for the unique optimal trajectory.**

I. Introduction

The present paper addresses a class of dual spacecraft sparse aperture interferometers. Such formations have been discussed previously in the literature. See for example [1]. This class of formations is chiefly motivated by NASA's Origins mission [2]. The formation is composed of two spacecraft (see Figure (1).) Both collect incoming light but only one, called the combiner spacecraft, combines the two collected beams and performs the interference process. While the combiner is fixed in space, the collector is proposed to evolve on a virtual paraboloid, whose axis of symmetry coincides with the common formation line of sight, in three dimensional space. The paraboloid results in improved focusing properties for the constellation [1].

Moreover, in [3], the authors treat a planar dual-spacecraft formation where the collector evolves along a linear spiral relative to the fixed combiner. Such a spiral maneuver results in complete coverage of a desired region in the frequency (u-v) domain called the resolution disk $\mathcal{D}_R$, which will be defined in Section (II). Combining these two constraints such that the collector spacecraft evolves on a spiral embedded on the paraboloid should result in both improved focusing properties as well as improved signal content (the effect of covering the u-v plane using a spiral maneuver).

This research is supported by NSF grants DMS-0103895, DMS-0305837 and CMS-0408542.

Islam Hussein, Aerospace Engineering, University of Michigan, Ann Arbor, ihussein@umich.edu.

Anthony Bloch, Professor of Mathematics, Mathematics Department, University of Michigan, Ann Arbor, abloch@umich.edu.

Daniel Scheeres, Associate Professor of Aerospace Engineering at the University of Michigan, Ann Arbor, scheeres@umich.edu.

Harris McClamroch, Professor of Aerospace Engineering, University of Michigan, Ann Arbor, nhm@umich.edu.

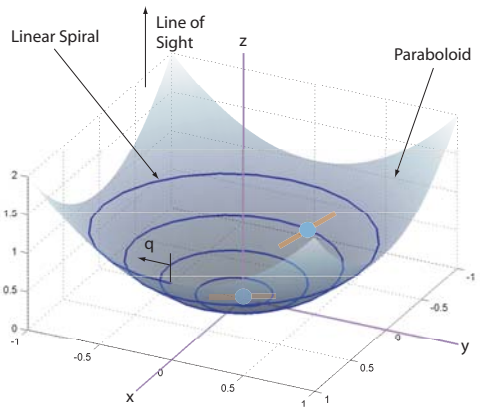

Fig. 1. The basic interferometer.

A third important consideration to take into account is signal-to-noise ratio (SNR) of the reconstructed image. It is desired that all frequencies in $\mathcal{D}_R$ be sampled while maximizing SNR. SNR can be controlled by controlling the relative speed (projected on the observation plane, which is perpendicular to the line of sight) between the spacecraft in the formation [4], [5]. As the projected relative speed between the spacecraft pair is minimized, the achievable SNR is maximized. Intuitively, as a spacecraft moves more slowly, it spends more time in the neighborhood of a relative position state in space. This leads to more photon collection from that neighborhood, resulting in a stronger signal.

The above provides a guideline for the formulation of an optimal control problem. The problem we consider is slightly different than the τ-elastic variational or the dynamic coverage problems considered in [5], [6], [7] in that it is a restricted version of these problems to handle the dual-spacecraft formation described above. The spacecraft are modeled as point particles. With the combiner spacecraft fixed at the focus of the paraboloid, the collector is constrained to move along a spiral embedded on a paraboloid, which is a one dimensional manifold. Hence, the system possesses only a single degree of freedom, which is the motion on the one dimensional manifold. SNR is taken into account by attempting to minimize a cost functional that is a weighted sum of the projected relative speed and fuel. The goal is to solve for the time parametrization of the control vector that minimizes the cost functional and reconstruct the time history of the collector spacecraft's traversal of the

spiral curve embedded on the manifold.

Here is how the paper is organized. In Section (II), we briefly describe the various aspects of image reconstruction. In Section (III), we give a general description of the model and define the various variables. With this done, we are in a position to define the optimal control problem and derive the necessary optimality conditions. These necessary conditions are shown to also be sufficient by proving that the problem is strictly convex. Strict convexity guarantees that a solution of the optimality conditions is in fact unique. This is done in Section (IV). In Section (V), we apply a continuation method to solve the necessary and sufficient conditions and verify that, indeed, they are solutions by showing that the Hamiltonian is constant along the trajectory. This furnishes the unique optimal trajectory. We conclude with some final remarks on future work in Section (VI).

II. Imaging and the Coverage Problem

In this section we review the various aspects of multi-spacecraft imaging. The discussion is for a generic formation of any number of spacecraft. In later sections, we specialize the discussion to dual spacecraft interferometry. Consider a formation of N spacecraft. Let $\mathbf{q}_i$ denote the coordinates of the i^{th} spacecraft, $i \in \mathcal{I} = \{1, \dots, N\}$. For later development, assume that $\mathbf{q}_i$ belongs to some one- or two-dimensional continuously differentiable manifold M embedded in $\mathbb{R}^3$. Also let $\mathbf{p}_i = (x_i, y_i, z_i)$ denote the position of the i^{th} spacecraft in $\mathbb{R}^3$. In general, we have

$$\mathbf{p}_i = (x_i, y_i, z_i) = \mathbf{f}(\mathbf{q}_i), \tag{2.1}$$

where $\mathbf{f} : M \to \mathbb{R}^3$ is a continuously differentiable mapping.

Let $O = \mathbb{R}^2$ be the observation plane (see Figure (1). The observation plane is a plane perpendicular to the line of sight (which we assume to be along the z-direction in $\mathbb{R}^3$) and whose origin coincides with the point $(0, 0, 0)$ (that is, the origin of $\mathbb{R}^3$). Assume that the maximum displacement along the line of sight of any spacecraft in the formation is bounded above by ε. That is to say $z_i < \varepsilon$. Let $\bar{z}$ denote the range from the observation plane to the target to be imaged. One can show that if $\varepsilon \ll \bar{z}$, then any inter-spacecraft offset along the line of sight between the spacecraft in the formation does not affect the quality of the reconstructed image [4]. Since the goal in the Origins program is to reconstruct images of extra-solar objects, the assumption that $\varepsilon \ll \bar{z}$ is valid.

Hence, in extra-solar interferometric imaging, we are interested in the relative position dynamics as projected onto the observation plane O. We are therefore interested in the projected relative trajectories:

$$\tilde{\mathbf{p}}_{ij}(t) = \mathbb{P}\left(\mathbf{q}_j(t) - \mathbf{q}_i(t)\right), \tag{2.2}$$

where $\tilde{\mathbf{p}}_{ij} : [0, T] \to O$ are curves on O and $\mathbb{P}$ is the mapping that projects relative trajectories on M onto the observation plane O. Note that $\mathbb{P} = \mathbb{P}_{xy} \circ \mathbf{f}$, where $\mathbb{P}_{xy} : \mathbb{R}^3 \to \mathbb{R}^2$ is a projection mapping with matrix representation

$$\begin{bmatrix} 1 & 0 & 0 \\ 0 & 1 & 0 \end{bmatrix}. \tag{2.3}$$

In multi-aperture interferometry, there are two main imaging goals. The first is simply referred to as frequency domain (or u-v plane) coverage. Here, we only state the coverage goal and refer the reader to [4] for a more detailed discussion. We are interested in having the resolution disc as defined by the set $\mathcal{D}_R = \left\{(u, v) : \sqrt{u^2 + v^2} \leq 1/\theta_r\right\}$ completely covered by some ball of radius r_p centered at $\lambda\tilde{\mathbf{p}}_{ij}(t)$, for some $t \in [0, T]$, i and j, where θ_r is the angular resolution and λ is the wavelength of the electromagnetic signal of interest. An image is said to be successfully completed if a maneuver $\mathcal{M}$ satisfies the following condition.

Definition II.1. (**Successful Imaging Maneuver**) An imaging maneuver $\mathcal{M}$ is said to be successful if, for each $(u, v) \in \mathcal{D}_R$, there exists a time $t \in [0, T]$ and some $i, j = 1, \dots, N$ such that $(u, v) \in \bar{B}_{r_p}\left(\lambda\tilde{\mathbf{p}}_{ij}(t)\right)$, where $\bar{B}_x(\mathbf{y})$ is a *closed* ball in $\mathbb{R}^2$ of radius x centered at $\mathbf{y}$. r_p is proportional to the size of the telescope's airy disc.

The second objective is that all frequencies in $\mathcal{D}_R$ must be sampled while maximizing the signal-to-noise ratio (SNR). SNR can be controlled by controlling the relative speeds between the spacecraft in the formation [4]. As the projected relative speed, denoted by $\|\dot{\tilde{\mathbf{p}}}_{ij}\|$, between a spacecraft pair is minimized, SNR is maximized. Intuitively, as a spacecraft moves more slowly, it has more time spent in the neighborhood of a relative position state in space. This leads to more photon collection at that state, which results in a stronger signal.

III. A Class of Dual-Spacecraft Interferometers

In this section we state the two constraints imposed on the collector spacecraft and derive the equations of motion of the collector spacecraft in terms of a single coordinate.

A. The Paraboloid Virtual Surface

The combiner spacecraft carries the ability to delay any wavefront it receives in its own aperture by an amount equal to twice the distance to the center of the paraboloid, thus simulating the delay for a ray that passes through the focus and reflects back to it. The collector spacecraft flies anywhere along the paraboloidal surface, carrying a mirror that reflects a second segment of the wavefront to the combiner at the focus, which then interferometrically combines the light from the two received apertures to synthesize a baseline equal to the perpendicular separation of the two spacecraft. In brief, the main reason for a paraboloid surface choice for the collector spacecraft is that a plane wavefront reflecting off a paraboloidal surface will come to a common focus. In cartesian coordinates a paraboloidal surface is given by:

$$z = \frac{1}{2}\left(\frac{\rho^2}{\beta^2} - \beta^2\right), \tag{3.1}$$

where $\rho = \sqrt{x^2 + y^2}$ and β is a parameter that controls the depth of the paraboloid. Note that vertex of the paraboloid is located at the point $(0, 0, -\beta^2/2)$.

B. The Spiral Maneuver

In the x-y plane, the projected position may be given in terms of polar coordinates (ρ, θ). One way to ensure full coverage of the resolution disc $\mathcal{D}_R$ is to initialize the second spacecraft such that at $t = 0$ we have $(\rho = \frac{1}{\theta_p}, \theta = 0)$, make it follow a linear spiral as a function of θ, and to impose the terminal condition that at $t = T$ we have $\rho = \frac{(m+1)}{2\theta_p}, \theta = \frac{(m-1)\pi}{2}$), where T is the terminal maneuver time. The number m is an integer that is equal to the number of pixels in the reconstructed image and θ_p is a parameter such that $\theta_p = m\theta_r$. This motion implies that the two coverage balls $\bar{B}_{r_p}(\tilde{\mathbf{p}}_{12})$ and $\bar{B}_{r_p}(\tilde{\mathbf{p}}_{21})$ are initialized such that they lie outside the central (fixed) ball $\bar{B}_{r_p}(\tilde{\mathbf{p}}_{00}) = \bar{B}_{r_p}(0, 0)$ and move spirally outwards till they lie outside the resolution disc $\mathcal{D}_R$. Thus ρ and θ must satisfy

$$\rho(\theta) = k(\pi + \theta), \ \theta \in \left[0, \frac{(m-1)\pi}{2}\right], \tag{3.2}$$

where $k = \frac{\lambda}{\pi\theta_p}$. Note that in general we take $\theta \in [0, \infty)$ and not restrict it to the set $[0, 2\pi)$.

Figure (2) shows an example of a trajectory in the physical and u-v planes for an object that is located at $\bar{z} = 15$pc (1pc$= 3.085 \times 10^{13}$km), with a field of view that is $\bar{L} = 12,760$km wide, with $m = 17$ pixels and, thus, a pixel size of $L = 750.6$km (i.e. the constellation is capable of detecting any object whose size is greater than L.) These values correspond to applications such as JPL's Terrestrial Planet Finder (TPF, [8]) and they could also be adjusted for Earth imaging applications. For more details on the spiral maneuver, we refer the reader to the papers [9] and [3] and references therein. As shown in Figure (2), the spiral maneuver is capable of entirely covering the resolution disc $\mathcal{D}_R$, which results in a successful maneuver.

C. Equations of Motion

Since we have a single spacecraft to control, the number of spacecraft $N = 1$. Enforcing the constraints (3.1) and (3.2) one finds that the position of the collector spacecraft in terms of the angular position θ is given by:

$$\mathbf{p}(\theta) = (x, y, z) = \left((k(\pi+\theta)\cos\theta, k(\pi+\theta)\sin\theta, \frac{1}{2}\left(\frac{k^2}{\beta^2}(\pi+\theta)^2 - \beta^2\right)\right). \tag{3.3}$$

We will use the arc length q traversed along the spiral as the single global coordinate on the one-dimensional manifold M. The arc length q is obtained as a function of θ using the definition of the arc length of a curve in space:

$$q(\theta) = h(\theta) = \int_0^\theta \left\| \frac{\partial \mathbf{p}(\theta')}{\partial \theta'} \right\| \mathrm{d}\theta',$$

where

$$\frac{\partial \mathbf{p}}{\partial \theta} = [k\cos\theta - k(\pi+\theta)\sin\theta]\,\mathbf{e}_x + [k\sin\theta + k(\pi+\theta)\cos\theta]\,\mathbf{e}_y + \left[\frac{k^2(\pi+\theta)}{\beta^2}\right]\mathbf{e}_z, \tag{3.4}$$

where $\mathbf{e}_x$, $\mathbf{e}_y$ and $\mathbf{e}_z$ denote unit vectors in the x, y and z directions, respectively. By the geometry of the problem described in previous paragraphs, it is easy to see that the function h is both one-to-one and onto. Hence, given a value for q, one can uniquely solve for θ using

$$\theta = h^{-1}(q). \tag{3.5}$$

Although one can obtain $h(\theta)$ explicitly in terms of θ (we omit it here due to space restrictions), there does not seem to be an analytic expression for h^{-1}.

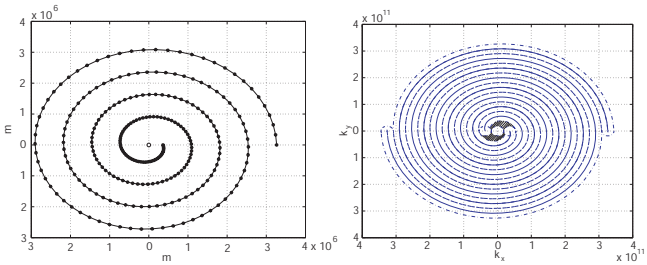

Fig. 2. Motion in the physical (in meters, left) and wave number (dimensionless, right) planes

Let $\mathbf{e}_t$ and $\mathbf{e}_n$ denote the unit vectors tangent and normal unit vectors at a point $q(t) \in M$, respectively. If we let $\mathbf{v} = v\mathbf{e}_t = \dot{q}\mathbf{e}_t$ denote the velocity of the collector spacecraft, $\mathbf{a} = a_t\mathbf{e}_t + a_n\mathbf{e}_n$ its acceleration and $\mathbf{u} = u_t\mathbf{e}_t + u_n\mathbf{e}_n$ the thrust vector applied to the collector, then the equations of motion are written in path-variable form as (see [10]):

$$\dot{q} = v, \ \dot{v} = u_t, \tag{3.6}$$

where we assume a unit mass for the collector spacecraft. Note that the normal component of the control vector is constrained to satisfy:

$$u_n = a_n = \frac{v^2}{R(\theta)}, \tag{3.7}$$

where $R(\theta)$ is the radius of curvature of M expressed in terms of the polar angle location θ. R is given by $\frac{1}{R} = \left\| \frac{\mathrm{d}\mathbf{e}_t}{\mathrm{d}q} \right\| = \|(\mathrm{d}\mathbf{e}_t/\mathrm{d}\theta) \cdot (\mathrm{d}\theta/\mathrm{d}q)\|$. In terms of θ, we find that[1]

$$\frac{1}{R(\theta)} = \frac{r(\theta)\left[k^2(\pi+\theta)^2 + \beta^4\left(1 + (\pi+\theta)^2\right)\right]}{\sqrt{\beta^4\left(2 + (\pi+\theta)^2\right)^2 + k^2\left(1 + (\pi+\theta)^2\left(3 + (\pi+\theta)^2\right)\right)}}.$$

In computing the curvature, we have used:

$$\mathrm{d}q = r(\theta)\mathrm{d}\theta = \left\| \frac{\partial h}{\partial \theta} \right\| \mathrm{d}\theta, \tag{3.8}$$

where

$$r(\theta) = k\sqrt{1 + \left(1 + \frac{k^2}{\beta^4}\right)(\pi+\theta)^2}. \tag{3.9}$$

IV. Necessary and Sufficient Optimality Conditions

In this section we formulate an optimal control problem and use the Maximum Principle to derive the necessary conditions. We then show that the problem is convex and that the necessary optimality conditions are also sufficient.

[1] All symbolic computations were verified in Mathematica.

With the two constraints imposed on the collector spacecraft, we have achieved a successful maneuver (by virtue of the spiral constraint) and improved focusing properties (by virtue of the paraboloid constraint.) The only degree of freedom remaining is the time parametrization of $q(t)$. This is determined by solving an optimal control problem that results in the time parametrization that minimizes the speed and fuel expenditure of the collector spacecraft, which are the last two important criteria in the motion path planning problem for the dual-spacecraft interferometer.

The goal is to minimize the cost functional:

$$\mathcal{J} = \int_0^T \frac{1}{2}\langle \mathbf{u}, \mathbf{u}\rangle + \frac{\tau^2}{2}\langle \tilde{\mathbf{v}}, \tilde{\mathbf{v}}\rangle \, \mathrm{d}t \tag{4.1}$$

subject to the dynamics (3.6) and the boundary conditions:

$$q(0) = 0,\ v(0) = v_0,\ q(T) = q_T,\ v(T) = v_T, \tag{4.2}$$

where $q_T = h\left(\theta = \frac{(m-1)\pi}{2}\right)$. In Equation (4.1), $\tilde{\mathbf{v}} = \dot{\tilde{p}}$ is the projected velocity of the collector on the x-y plane and $\mathbf{u} = u_t\mathbf{e}_t + u_n\mathbf{e}_n$ is the total thrust vector. $\langle\cdot,\cdot\rangle$ denotes the Euclidean inner product defined on $\mathbb{R}^3$.

To compute $\tilde{\mathbf{v}}$ in terms of q and $\dot{q}$, we first need to obtain an expression for $\dot{\theta}$ in terms of q and $\dot{q}$. Differentiating Equation (3.4), we obtain

$$\dot{q} = r(\theta)\dot{\theta}, \tag{4.3}$$

where $r(\theta)$ is given by Equation (3.9). Using this and Equations (3.3) and (3.5), we have:

$$\tilde{\mathbf{v}} = \dot{x}\mathbf{e}_x + \dot{y}\mathbf{e}_y = P_x(\theta, v)\mathbf{e}_x + P_y(\theta, v)\mathbf{e}_y, \tag{4.4}$$

where

$$\begin{aligned} P_x(\theta, v) &= \frac{v}{r(\theta)}\left[k\cos(\theta) - k(\pi+\theta)\sin(\theta)\right] \\ P_y(\theta, v) &= \frac{v}{r(\theta)}\left[k\sin(\theta) + k(\pi+\theta)\cos(\theta)\right]. \end{aligned}$$

In fact, one can show that $\langle \tilde{\mathbf{v}}, \tilde{\mathbf{v}}\rangle = \frac{k^2v^2}{r^2(\theta)}\left[1 + (\pi+\theta)^2\right]$. Hence the cost is given by:

$$\frac{1}{2}u_t^2 + \frac{v^4}{2R^2(\theta)} + \frac{\tau^2}{2}\frac{k^2v^2}{r^2(\theta)}\left(1 + (\pi+\theta)^2\right). \tag{4.5}$$

We now apply the Maximum Principle to derive the necessary conditions. First define the pre-Hamiltonian:

$$\begin{aligned} \hat{H}(\theta, v, u_t, p_1, p_2) = &-\frac{1}{2}u_t^2 - \frac{v^4}{2R^2(\theta)} \\ &-\frac{\tau^2}{2}\frac{k^2v^2}{r^2(\theta)}\left(1 + (\pi+\theta)^2\right) + p_1 v + p_2 u_t, \end{aligned} \tag{4.6}$$

where p_1 and p_2 are the momentum variables. From the necessary condition $\frac{\partial \hat{H}}{\partial u_t} = 0$, we find that $u_t = p_2$. Substituting this into (4.6), we get the Hamiltonian function:

$$\begin{aligned} H(\theta, v, p_1, p_2) &= p_1 v + \frac{1}{2}p_2^2 - \frac{v^4}{2R^2(\theta)} \\ &\quad -\frac{\tau^2}{2}\frac{k^2v^2}{r^2(\theta)}\left(1 + (\pi+\theta)^2\right). \end{aligned} \tag{4.7}$$

The necessary conditions are given by:

$$\begin{aligned} \dot{q} &= \frac{\partial H}{\partial p_1} = v \ \Leftrightarrow\ \dot{\theta} = \frac{v}{r(\theta)} \\ \dot{v} &= \frac{\partial H}{\partial p_2} = p_2 \\ \dot{p}_1 &= -\frac{\partial H}{\partial q} = -\frac{1}{r(\theta)}\left[\frac{v^4}{R^3(\theta)}\frac{\partial R}{\partial \theta}\right. \\ &\quad \left. -\frac{\tau^2k^2v^2}{r^2(\theta)}(\pi+\theta) + \frac{\tau^2k^2v^2}{r^3(\theta)}\frac{\partial r}{\partial \theta}\left[1 + (\pi+\theta)^2\right]\right] \\ \dot{p}_2 &= -\frac{\partial H}{\partial v} = -p_1 + \frac{2v^3}{R^2(\theta)} + \frac{\tau^2k^2v}{r^2(\theta)}\left[1 + (\pi+\theta)^2\right]. \end{aligned} \tag{4.8}$$

We have used the fact that $\partial q/\partial\theta = r(\theta)$ and used the chain rule in computing the derivative of $r(\theta)$ and $R(\theta)$ with respect to q. We also used $\dot{q} = v = r(\theta)\dot{\theta}$ to obtain the necessary conditions in terms of (θ, v, p_1, p_2) (as given by the second equation on the first line,) which is more convenient to use in the computations in the next section since all equations are in terms of θ and not q.

We now show that the necessary conditions are also sufficient and that there exists a unique solution to the problem. This is done by showing that we have a strictly convex optimal control problem. First, we need the following standard result.

Lemma IV.1. *Let $f(x) = h(g(x)) : \mathbb{R} \to \mathbb{R}$, where $g : \mathbb{R} \to \mathbb{R}$ is concave and $h : \mathbb{R} \to \mathbb{R}$ is convex and non-increasing. Then $f(x)$ is convex.*

Proof Note that $f''(x) = h''(g')^2 + h'g''$, where the prime indicates the derivative with respect to the argument. Since g is concave, $g'' \le 0$ for all x in $\mathbb{R}$. Since h is convex, $h'' \ge 0$ and since it is non-increasing, $h' \le 0$ for all $x \in \mathbb{R}$. This shows that $f''(x) \ge 0$ for all $x \in \mathbb{R}$. Hence, $f(x)$ is convex for all $x \in \mathbb{R}$. ■

Strict convexity is obtained if h is strictly convex and strictly decreasing ($h''(x) > 0$ and $h'(x) < 0\ \forall\ x \in \mathbb{R}$) and $g(x)$ is strictly concave ($g''(x) < 0\ \forall\ x \in \mathbb{R}$.)

Since the dynamics (3.6) are linear and the variables q, v and u_t are all unconstrained (that is, $q, v, u_t \in \mathbb{R}$) and, hence, belong to trivially convex sets, we only need to show that the cost function in Equation (4.1) is strictly convex in q, v and u_t to guarantee sufficiency of the necessary conditions and uniqueness of the solution. Since the cost (4.5) is quadratic in u_t, it is strictly convex in u_t. It is also strictly convex in v since it is a sum of a quadratic and a fourth power of v (both are strictly convex and the sum of two strictly convex functions is also strictly convex).

What remains to show is that the cost (4.5) is convex in q. This is done by showing that $h_1(\theta) = 1/R^2(\theta)$ and $h_2(\theta) = (1+(\pi+\theta)^2)/r^2(\theta)$ are convex and non-increasing in θ and that $\theta = h^{-1}(q)$ is concave in q. Since the sum of two convex functions is also convex, then the q-dependent terms of the cost (4.5) is convex. First, note that:

$$\begin{aligned} h_1'(\theta) &= -\frac{\chi_1(\theta)}{k^2\left[k^2(\pi+\theta)^2 + \beta^4(1+(\pi+\theta)^2)\right]^4} < 0 \\ h_1''(\theta) &= \frac{\chi_2(\theta)}{k^2\left[k^2(\pi+\theta)^2 + \beta^4(1+(\pi+\theta)^2)\right]^5} > 0 \end{aligned}$$

for all $\theta \in [0, (m-1)\pi/2]$ where

$$\begin{aligned} \chi_1(\theta) = 2\beta^8(\pi+\theta)\Big[&\beta^8(2+(\pi+\theta)^2)(4+(\pi+\theta)^2) \\ &+ k^4(3+(\pi+\theta)^2(6+(\pi+\theta)^2)) \\ &+ 2\beta^4k^2(6+(\pi+\theta)^2(6+(\pi+\theta)^2))\Big] > 0, \end{aligned}$$

$$\chi_2(\theta) = 2\beta^8\Big[3k^6(\pi+\theta)^2(7+(\pi+\theta)^2(10+(\pi+\theta)^2)) + \beta^{12}(-8+(\pi+\theta)^2(2+(\pi+\theta)^2)(19+3(\pi+\theta)^2)) + \beta^8k^2(-12+(\pi+\theta)^2(104+(\pi+\theta)^2(80+9(\pi+\theta)^2))) + \beta^4k^4(-3+(\pi+\theta)^2(87+(\pi+\theta)^2(85+9(\pi+\theta)^2)))\Big] > 0$$

for all $\theta \in [0,(m-1)\pi/2]$. Hence, $h_1(\theta)$ is strictly convex and is strictly decreasing for all $\theta \in [0,(m-1)\pi/2]$. For h_1, first write it explicitly in θ:

$$h_2(\theta) = \frac{1+(\pi+\theta)^2}{k^2\left[1+\left(1+\frac{k^2}{\beta^4}\right)(\pi+\theta)^2\right]}.$$

The derivatives of h_2 are given by:

$$h_2'(\theta) = -\frac{2\beta^4(\pi+\theta)}{\left[k^2(\pi+\theta)^2+\beta^4(1+(\pi+\theta)^2)\right]^2} < 0$$

$$h_2''(\theta) = \frac{2\beta^4\left[3k^2(\pi+\theta)^2+\beta^4(-1+3(\pi+\theta)^2)\right]}{\left[k^2(\pi+\theta)^2+\beta^4(1+(\pi+\theta)^2)\right]^3} > 0$$

for all $\theta \in [0,(m-1)\pi/2]$. Hence, $h_2(\theta)$ is strictly convex and is strictly decreasing for all $\theta \in [0,(m-1)\pi/2]$. Finally, using Equation (3.8), we have

$$\frac{\mathrm{d}\theta}{\mathrm{d}q} = \frac{1}{r(\theta)}, \quad \frac{\mathrm{d}^2\theta}{\mathrm{d}q^2} = -\frac{1}{r^2(\theta)}\frac{\mathrm{d}r}{\mathrm{d}\theta}\frac{\mathrm{d}\theta}{\mathrm{d}q}.$$

Since, $\mathrm{d}\theta/\mathrm{d}q = 1/r$ and

$$\frac{\mathrm{d}r}{\mathrm{d}\theta} = \frac{k^2}{r(\theta)}\left(1+\frac{k^2}{\beta^4}\right)(\pi+\theta)$$

then we have

$$\frac{\mathrm{d}^2\theta}{\mathrm{d}q^2} = -\frac{k^2}{r^4(\theta)}\left(1+\frac{k^2}{\beta^4}\right)(\pi+\theta),$$

which is strictly negative for all $\theta \in [0,(m-1)\pi/2]$. This shows that $\theta = h^{-1}(q)$ is a strictly concave function of q for all value of θ in the desired range.

The above arguments show that we have a strictly convex problem since we have a strictly convex cost function and linear dynamics and since the space of candidate trajectories $(q(t),v(t),u_t(t)) \in \mathbb{R}^3$, which is trivially convex, for all $t \in [0,T]$. Based on the Corollary on page 214 and Theorem 10 on page 216 in [11], this gives the following result.

Theorem IV.1. *The necessary conditions (4.9) are also sufficient and have a unique global optimal solution.*

V. Numerical Solution

In this section we numerically obtain the unique solution to the necessary and sufficient conditions given by Equations (4.9). We use MATLAB's bvp4c.m function, the two-point boundary value problem solver. This uses a simple shooting method that requires an initial guess for the time parameterized states: $q(t)$ (or $\theta(t)$), $v(t)$, $p_1(t)$ and $p_2(t)$. Since an initial guess is hard to obtain, we use continuation method (homotopy) to solve the problem (see Chapter 7 in [12]). This is done as follows.

We now derive the necessary conditions for the modified cost functional. The goal is to minimize the cost functional:

$$\mathcal{J}_\varepsilon = \int_0^T \frac{1}{2}u_t^2 + \frac{\varepsilon}{2}\left[\frac{v^4}{R^2(\theta)} + \frac{\tau^2k^2v^2}{r^2(\theta)}\left(1+(\pi+\theta)^2\right)\right]\mathrm{d}t. \tag{5.1}$$

For this cost function, the Hamiltonian is given by:

$$H_\varepsilon(\theta,v,p_1,p_2,\varepsilon) = p_1v + \frac{1}{2}p_2^2 - \frac{\varepsilon}{2}\left[\frac{v^4}{R^2(\theta)} + \frac{\tau^2k^2v^2}{r^2(\theta)}\left(1+(\pi+\theta)^2\right)\right]. \tag{5.2}$$

The necessary conditions are given by:

$$\begin{aligned}
\dot{q} &= v \\
\dot{v} &= p_2 \\
\dot{p}_1 &= -\frac{\varepsilon}{r(\theta)}\left[\frac{v^4}{R^3(\theta)}\frac{\partial R}{\partial\theta} - \frac{\tau^2k^2v^2}{r^2(\theta)}(\pi+\theta) + \frac{\tau^2k^2v^2}{r^3(\theta)}\frac{\partial r}{\partial\theta}\left[1+(\pi+\theta)^2\right]\right] \\
\dot{p}_2 &= -p_1 + \varepsilon\left[\frac{2v^3}{R^2(\theta)} + \frac{\tau^2k^2v}{r^2(\theta)}\left(1+(\pi+\theta)^2\right)\right].
\end{aligned} \tag{5.3}$$

Note that these are still sufficient and that the solution is unique for each $\varepsilon \in [0,1]$. For $\varepsilon = 0$ we have:

$$\dot{q} = v,\ \dot{v} = p_2,\ \dot{p}_1 = 0,\ \dot{p}_2 = -p_1,$$

which now form a set of linear differential equations. One can easily solve these differential equations to obtain:

$$\begin{aligned}
q(t) &= v_0t - \frac{t^3}{6}p_1^0 + \frac{t^2}{2}p_2^0 \\
v(t) &= v_0 - \frac{t^2}{2}p_1^0 + tp_2^0 \\
p_1(t) &= p_1^0 \\
p_2(t) &= -tp_1^0 + p_2^0,
\end{aligned} \tag{5.4}$$

where p_1^0 and p_2^0 are constants given by:

$$\begin{aligned}
p_1^0 &= -\frac{6}{T^2}(v_T+v_0) + \frac{12}{T^3}q_T \\
p_2^0 &= \frac{6}{T^2}q_T - \frac{2}{T}v_T - \frac{4}{T}v_0
\end{aligned}$$

and where q_T, v_0 and v_T are the boundary conditions.

In a continuation method, one uses the solution to the problem with $\varepsilon = \varepsilon_0 = 0$ (that is, Equations (5.4)) as the initial guess for $\varepsilon_1 = \delta$, where δ is a sufficiently small parameter. Assuming that the problem with $\varepsilon = \varepsilon_1 = \delta$ has been successfully solved, one then uses this solution as the initial guess for the next step with, say, $\varepsilon = \varepsilon_2 = 2\delta$. This is repeated until $\varepsilon = \varepsilon_j = j\delta$ is sufficiently close to $\varepsilon = 1$. At this point, we are able to solve the two point boundary value problem (5.3) with $\varepsilon = 1$, which corresponds to the original problem (4.9) we are seeking to solve.

Consider the optimal control problem with $\tau = 10$, $\beta = 10$, $T = 1000$ seconds, $q_0 = 0$, $q_T = 5.26 \times 10^5$ km, $v_T = v_0 = 0$ m/s and using the same values used to generate Figure (2) which give $k = 1.154 \times 10^4$. The continuation method is applied starting with the explicit solution (5.4) (corresponding to $\varepsilon = 0$) with a step size of $\delta = 0.01$. The result is shown in Figure (3). In the figure, we plot the solution with $\varepsilon = 0$, $\varepsilon = 0.33$, $\varepsilon = 0.50$, $\varepsilon = 0.67$ and $\varepsilon = 1.0$, which corresponds to the desired solution to our problem. To show that, indeed, the solution is continuous in ε, $q(t)$ and $v(t)$ are plotted in on the right in Figure (3) for $t \le 100.01$ seconds. One can now see that the solution varies smoothly as a function of ε.

As a final check on the numerical solutions shown in

Figure (3), the Hamiltonian H_ε must be constant along the motion for every value of ε. Evaluating H_ε for the different values of ε, we get $H_{\varepsilon=0}(t) = 4.982 \times 10^6$ (with 0% deviation from the mean value since this is the exact solution), $H_{\varepsilon=0.33}(t) = 3.74 \times 10^8$ (0.22% deviation), $H_{\varepsilon=0.5}(t) = 5.57 \times 10^8$ (0.23% deviation), $H_{\varepsilon=0.67}(t) = 7.40 \times 10^8$ (0.25% deviation) and $H_{\varepsilon=1}(t) = 1.09 \times 10^9$ (0.26% deviation) on average for all values of time $t \in [0, 1000]$. The small perturbations in the values of the Hamiltonian is attributed to numerical errors involved in the computation, where we note that as ε is increased, the $\%$ error increases. The Hamiltonian is plotted in Figure (4).

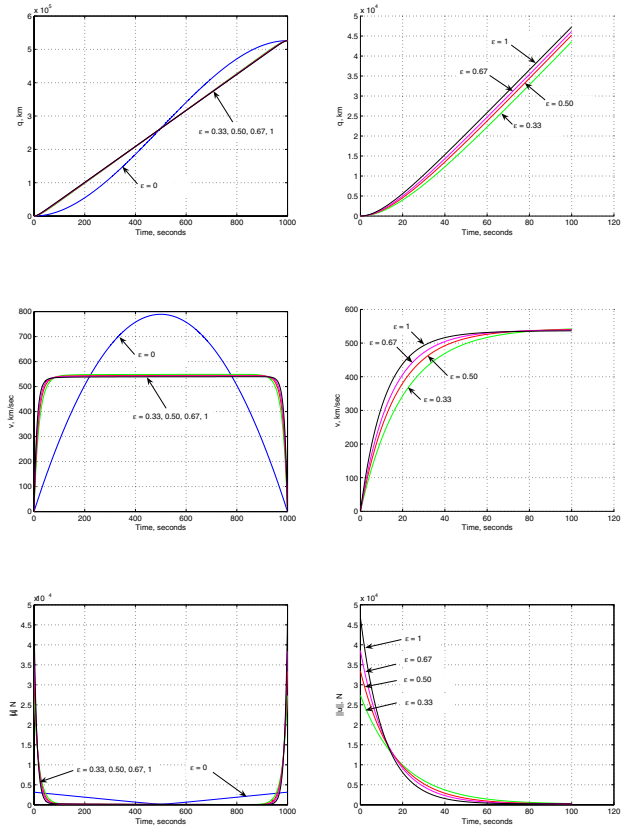

Fig. 3. $q(t)$, $v(t)$ and $\|u(t)\|$ for $\varepsilon = 0$ (exact solution), $\varepsilon = 0.33$, $\varepsilon = 0.50$, $\varepsilon = 0.67$ and $\varepsilon = 1.00$, which is the desired solution for the optimal control problem: for $t \in [0, T]$ (left) and $t \leq 1.401$s (right.)

VI. Conclusion

In this paper, we introduced the main elements of formation flying for imaging applications, including the coverage problem. We then specialized the discussion to a two spacecraft formation introduced previously in the literature. The first main contribution of this paper is that we combined two ideas introduced separately in the literature and proposed a maneuver that guarantees full coverage of the u-v plane (the spiral) and improved focusing properties (the paraboloid). The geometry of the problem was described and the governing dynamic equations derived. We then formulated an optimal control problem that aims to minimize a cost functional composed of a weighted sum of fuel expenditure and the projected relative speed. This cost function is chosen to both reduce mission fuel costs and improve image quality by increasing SNR.

The necessary conditions were derived and were shown to be sufficient and to have a unique solution. We used a continuation procedure to solve the resulting two point boundary value problem for the unique solution. Current work will use the image quality performance index used in [3] to evaluate the performance of the solution found in the present paper and compare the results with those obtained previously in [3].

VII. Acknowledgements

The authors wish to thank Professor Peter Gorham, who contributed to Section (III-A) of this paper.

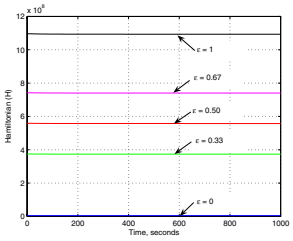

Fig. 4. Hamiltonian for the cases $\varepsilon = 0$, $\varepsilon = 0.33$, $\varepsilon = 0.50$, $\varepsilon = 0.67$ and $\varepsilon = 1.00$.

References

[1] P. W. Gorham, W. M. Folkner, and G. H. Blackwood, "Enabling concepts for a dual spacecraft formation-flying optical interferometer for NASA's ST3 mission," *Proc. of the 1999 Dana Pt. Conf. on Optical Interferometry*, vol. 194, p. 359, 1999.

[2] NASA, "Nasa origins program," URL: http://origins.jpl.nasa.gov, 2003.

[3] I. I. Hussein, D. J. Scheeres, and D. C. Hyland, "Control of a satellite formation for imaging applications," *Proceedings of the 2003 American Control Conference*, pp. 308–313, June 2003.

[4] S. Chakravorty, "Design and optimal control of multi-spacecraft interferometric imaging systems," Ph.D. dissertation, Aerospace Engineering, University of Michigan, 2004.

[5] I. I. Hussein and A. M. Bloch, "Dynamic interpolation on Riemannian manifolds: An application to interferometric imaging," *Proc. of the 2004 American Control Conference*, pp. 413–418, July 2004.

[6] ——, "Dynamic coverage optimal control for interferometric imaging spacecraft formations," *43rd IEEE Conference on Decision and Control*, December 2004, to appear.

[7] ——, "Optimal control on Riemannian manifolds with potential fields," *43rd IEEE Conference on Decision and Control*, December 2004, to appear.

[8] *The Terrestrial Planet Finder: A NASA Origins Program to search for habitable planets*. Jet Propulsion Laboratory Publication 99-003, May 1995.

[9] I. I. Hussein, D. J. Scheeres, and D. C. Hyland, "Formation path planning for optimal fuel and image quality for a class of interferometric imaging missions," *2003 AAS/AIAA Space Flight Mechanics Meeting*, February 9–13 2003.

[10] J. H. Ginsberg, *Advanced Engineering Dynamics*. Cambridge, United Kingdom: Cambridge University Press, 1998.

[11] E. B. Lee and L. Markus, *Foundations of Optimal Control Theory*. New York, NY: John Wiley & Sons, Inc., 1967.

[12] V. I. Shalashilin and E. B. Kuznetsov, *Parametric Continuation and Optimal Parametrization in Applied Mathematics and Mechanics*. Dordrecht, The Netherlands: Kluwer Academic Publishers, 2003.